Title
NEW ASPECTS OF HIGH ENERGY HEAVY-ION TRANSFER REACTIONS

Author
Scott, David K.

Publication Date
1975-03-01

Presented at the International Conference
on Cluster Structure of Nuclei and
Transfer Reactions Induced by Heavy Ions,
Tokyo, Japan, March 17 - 22, 1975

LBL-3495
c.1

NEW ASPECTS OF HIGH ENERGY HEAVY-ION TRANSFER REACTIONS

David K. Scott

March 1975

Prepared for the U. S. Energy Research and
Development Administration under Contract W-7405-ENG-48

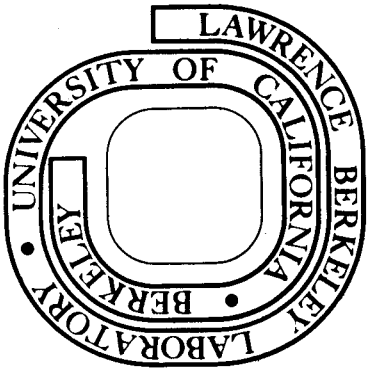

LBL-3495
c.1

DISCLAIMER

NEW ASPECTS OF HIGH ENERGY HEAVY-ION TRANSFER REACTIONS

LBL-3495

David K. Scott

Lawrence Berkeley Laboratory
University of California
Berkeley, California 94720

1. Introduction

The studies of heavy-ion reactions at incident energies in the region of 10 MeV/nucleon, though relatively few, have already led to a variety of new phenomena in nuclear structure and nuclear reaction mechanisms. In discussing these new aspects a key role is played by the peripheral nature of the collisions, which leads to simplicities in the differential cross-sections. First we gain insight into these simplicities by following complementary quantum mechanical and semi-classical approaches. The distortion of the peripheral distribution through the interference of direct and multistep processes is used to illustrate aspects of high energy reactions unique to heavy-ions. The simplicities of the distributions for reactions on lighter nuclei are exploited to give new information about nuclear structure from direct and compound reactions at high energy.

2. Differential Cross Sections for Peripheral Reactions

In general the scattering amplitude can be written.[0,1,2,3,4]

$$f(\Theta) = \frac{1}{2ik} \sum (2\ell+1)\ \eta_\ell\ e^{2i\delta_\ell}\ P_\ell(\cos\Theta) \qquad (1)$$

Assuming a peripheral collision, we can write the reaction amplitude (justified by the output of "exact" DWBA calculations; see Fig. 2(a)):

$$\eta_\ell = \eta_{\ell o}\ \ \mathrm{EXP}\ \ -\left[\frac{(\ell-\ell_o)^2}{(\Delta\ell)^2}\right] \qquad (2)$$

where ℓo corresponds to the grazing trajectory, and $\Delta\ell$ is the range of contributing partial waves. For δ_ℓ we make a Taylor expansion:

$$\delta_\ell = \delta_{\ell o} + \left(\frac{d\delta}{d\ell}\right)_{\ell o} (\ell-\ell o) + 1/2 \left(\frac{d^2\delta}{d\ell^2}\right)_{\ell o} (\ell-\ell o)^2 + \ldots\ldots\ldots \quad (3)$$

On account of the W.K.B. relationship between scattering angle Θ_ℓ corresponding to partial wave ℓ,

$$\Theta_\ell = 2\,\frac{d\delta_\ell}{d\ell} \quad (4)$$

we can write:

$$\delta_\ell = \delta_{\ell o} + \left(\frac{\Theta_o}{2}\right) (\ell-\ell o) + 1/4 \left(\frac{d\Theta\ell}{d\ell}\right)_{\ell o} (\ell-\ell o)^2 + \ldots\ldots\ldots \quad (5)$$

where Θ_o is the angle of the grazing trajectory. Assuming a peripheral collison at high incident energy, viz. $\ell o \gg \Delta\ell \gg 1$, we can use the asymptotic form for P_ℓ and convert the summation to an integral, to yield:

$$\frac{d\sigma}{d\Omega} = |f(\Theta)|^2 \;\alpha\; \text{EXP}\left[\frac{-(\Theta-\Theta_o)^2}{(\Delta\Theta)^2}\right] + \text{EXP}\left[\frac{-(\Theta+\Theta_o)}{(\Delta\Theta)^2}\right] + \begin{matrix}\text{INTERFERENCE}\\ \text{TERM}\end{matrix} \quad (6)$$

This equation can be interpreted[2] as the superposition of two classical distributions centered at Θ_o and $-\Theta_o$ and a resultant interference, which for high energy reactions can often be ignored, leaving us to consider the "physical" distribution centered at Θ_o. This represents a symmetric distribution of width:

$$(\Delta\Theta)^2 = \frac{2}{(\Delta\ell)^2} + 1/2 \left(\frac{d\Theta_\ell}{d\ell}\right)^2 (\Delta\ell)^2 \quad (7)$$

Using the classical relation for Rutherford scattering, $\ell=\eta\,\cot(\Theta/2)$, gives $(d\Theta_\ell/d\ell)_{\ell o} = 0.013$ for the reaction of 78 MeV ^{12}C ions on ^{144}Nd, enabling

us to construct the $\Delta\ell$ vs. $\Delta\Theta$ curve in Fig. 1. The curve has a minimum at $\Delta\ell = \sqrt{2(d\ell/d\theta)_{\ell_o}} = \sqrt{\eta}$ cosec $(\theta_o/2) \approx 12$ for the above reaction. For larger $\Delta\ell$ values we have a classical situation and $\Delta\Theta$ increases with $\Delta\ell$, whereas for small $\Delta\ell$ values the situation is quantum mechanical with $\Delta\Theta$ increasing as $\Delta\ell$ decreases. Shown on the figure is the $\Delta\ell$ value derived from a quantum mechanical DWBA calculation of the ^{144}Nd(^{12}C,^{13}C)^{143}Nd reaction, and the resulting value of $\Delta\Theta = 9.2^\circ$ is close to the observed half-width at 1/e of the maximum (See Fig. 2(a)). These one-nucleon trasfer data are therefore well described by the above treatment. Because the data correspond to the minimum of the $\Delta\ell$ vs. $\Delta\Theta$ curve, the width of the peripheral maximum is relatively stable against variations of $\Delta\ell$. This effect is illustrated in the figure by comparing calculations with different optical potentials (see figure caption) which give almost identical results for the classical maximum.

Such is not the case for the two-neutron transfer reaction ^{144}Nd(^{12}C,^{14}C)^{142}Nd illustrated in 2(b). Here a change in the radius parameter of the imaginary potential from 1.26 → 1.36 fm changes the forward cross section by a factor of 10. The corresponding reaction amplitudes for these cases are shown in Fig. 3(a). In neither case does the value of $\Delta\Theta$ predicted from Fig. 1 approach the observed width of the two-neutron transfer distribution. Furthermore the maximum for this case is less well-defined and has a pronounced asymmetry.

This asymmetry can be accounted for by carrying the expansion of δ_ℓ in Equ. 3 to the next order[2]:

$$\delta_\ell = \delta_{\ell o} + \left(\frac{\theta_o}{2}\right)(\ell-\ell_o) + \ldots\ldots\ldots + 1/3\ \beta\ (\ell-\ell_o)^3 \qquad (8)$$

The resultant differential cross section becomes tipped to forward angles, while the effect on the deflection function becomes:

$$\Theta_\ell = 2\frac{d\delta_\ell}{d\ell} = \Theta_o + \ldots\ldots\ldots + \beta\,(\ell-\ell_o)^2 \qquad (9)$$

i.e. a "parabolic dip" is added. We illustrate this effect by computing an "optical-model deflection function" from the derivative with respect to ℓ of the DWBA phase shifts. As shown in Fig. 3(b), the potential which generates the asymmetric distribution has a dip in the center of the ℓ-window. This dip was not evident in the deflection function for one-nucleon transfer. These results reflect the sharper fall-off of the two-nucleon form factor and the greater sensitivity of the forward cross section to close trajectories in the semiclassical picture. A comparison of one- and two-nucleon transfer can be used to probe the nuclear edge and the relationship of the real and imaginary potentials.[5]

This approach was used by Strutinskii a long time ago[1] as a guide to the understanding of high energy heavy-ion angular distributions. In that treatment the expansion in Equ. 3 was carried out to first order so that the increasing dispersion in Θ with increasing $\Delta\ell$ was not accounted for, but the evaluation of the differential cross sections can be parameterised by $\Theta_g(\Delta\ell)$, as shown in Fig. 4(a). The curves bear a striking resemblance to the experimental data for one-proton transfer induced by 389 MeV Argon ions on ^{232}Th on the right,[6] where there is a transition from the peripheral maximum at low excitation energy to the forward rising cross sections of the deeply inelastic region. This effect is currently being interpreted in terms of frictional, transport or relaxation phenomena.[7] It will be interesting to see if these models relate to $\Theta_g(\Delta\ell)$ in the above way. So far it has proved difficult to parameterize all the experimental distributions using only the Gaussian

form for reaction amplitudes and the expansion of δ_ℓ to 2nd order.[6] However, as our discussion of the Nd data for one- and two-nucleon transfer showed, it may well be necessary to carry out the expansion to higher orders. A similar conclusion may be implicit in the work of Kohno et al., discussed at this conference.

Fig. 4(a) shows clearly that the differential cross section evolves from bell-shaped semiclassical maximum (for $\Theta_g \Delta\ell \approx 5$), to a monotonically decreasing curve ($\Theta_g \Delta\ell \approx 1$) and finally for $\Delta\ell = 0$ to a $1/\sin\Theta$ curve which is characteristic of the decay of a stationary state of the compound system with high angular momentum oriented perpendicular to the reaction plane. The next three sections exploit the above three categories to reveal several new facets of heavy-ion reactions.

3. Distortion of Peripheral Maximum by Multistep Interferences

We consider the two-neutron transfer reactions $(^{18}O, ^{16}O)$, $(^{16}O, ^{18}O)$ on Sn isotopes at approximately 100 MeV. From the value of $\Theta_g \Delta\ell \approx 5$, we expect the distributions to have a classical maximum with the possible asymmetry discussed in the last section. The differential cross sections for the $^{120}Sn(^{18}O, ^{16}O)^{122}Sn$ and $^{122}Sn(^{16}O, ^{18}O)^{120}Sn$ reactions are shown in Fig. 5 for the g.s and 2^+ vibrational states.[8] The distributions for the ground states are almost identical and have a bell-shaped maximum as does the distribution for the 2^+ state in the pick-up reaction. The 2^+ distribution in stripping however is anomalous, becoming almost flat at forward angles. This effect cannot be reproduced by adjustment of the optical potential as discussed in the previous section, while obtaining a fit to the other distributions simultaneously.

The origin of the anomaly in this case lies in interferences between direct and indirect routes,[10] illustrated in Fig. 6. In the production of the 2^+ state, transitions 1 and 4 are segments of indirect paths and are common to both the stripping and pick-up processes, while 2 is the direct transition for pick-up and 3 for stripping, The amplitudes for these last two transitions have opposite sign according to the microscopic theory of vibrational states. The opposite sign leads to constructive interference between direct and indirect modes for the pick-up reaction (O^{16},O^{18}) and destructive interference in the stripping $(^{18}O,^{16}O)$ reaction. The destructive interference between two amplitudes, both peaked near the grazing angle, leads to distortion of the bell-shaped distribution while a constructive interference, retains the characteristic peak. That the two ground state cross sections are similar follows from the fact that these are time-reversed reactions (the center of mass energies being almost equal in the experiments). That they also retain the characteristic peripheral maximum, undistorted by higher order processes, can be understood from Fig. 6. In this case for either ground state transition both 2 and 3 enter the two lowest order indirect modes. Since they have opposite signs they tend to cancel each other resulting in negligible higher order contributions.

For the quantitative analysis of the effect with the coupled channels Born approximation (CCBA) we have derived the relevant optical model and deformation parameters from the elastic and inelastic (2^+) scattering of ^{16}O on ^{122}Sn. The theoretical fit to this data shown in Fig. 7 used optical model parameters V = 87.9 MeV, W = 24.24 MeV, $r_v = 1.203$, $r_w = 1.19$, $r_c = 1.20$, $a_v = 0.502$, $a_w = 0.67$, together with nuclear and charge deformations for ^{122}Sn of $\beta_N = 0.124$ $(R_N = 1.12(122)^{1/3})$ and $\beta_C = 0.095(R_C = 1.2(122)^{1/3})$. Here β_N

is close to the value obtained in proton inelastic scattering[11], and β_C is slightly reduced from the value 0.118 derived from the measured B(E2, 0 → 2).[12] For ^{120}Sn we follow a similar prescription, viz. $\beta_N = 0.13$ and β_C reduced from 0.112 (Ref. 12) to 0.09.

The theoretical predictions of CCBA theory for the stripping and pick-up reactions are shown in Fig. 5, which successfully reproduce the main features of the data discussed earlier. The absolute theoretical cross sections are also in remarkably good agreement with experiment since a factor of only 2.5 was required to normalize the theory to the data for the ground states. Heavy-ion reactions are rich in possibilities for studying the phenomenon not only in neutron transfers, but also in time-reversed proton transfers. These reactions may prove to be a sensitive means of probing inelastic modes, not directly observable, and ultimately of deformations and nuclear structure. The simplicity of the unperturbed differential cross section makes the effect particularly transparent in heavy-ion reactions.[13]

4. Reactions with Small $\Theta_g \Delta\ell$

For reactions between "light" heavy-ions at high energy, e.g. ^{12}C + ^{12}C at 10 - 15 MeV/nucleon, small values of $\Theta_g \Delta\ell \approx 1$ are encountered, leading as Fig. 4 shows to cross sections which fall monotonically with angle on the average. In certain cases, oscillations can be present and in fact the recent rediscovery of these oscillations has led to the widespread use in supplementing our knowledge of nuclear structure derived from light-ion reactions.[14] For multinuclean transfer, the differential cross sections often have the above featureless form, as illustrated by the collection of data[15,16] in Fig. 8, and serve as poor

signatures of J-value, although potentially it is just these reactions which are capable of yielding information on new types of correlation inaccessible in conventional light-ion reactions. For example it was recently shown that two and three-nucleon transfer reactions with heavy-ion beams of ≈ 10 MeV/nucleon are highly selective in exciting simple cluster configurations in light nuclei.[16] The discovery of these states is currently of interest to calculations using a folding model for three and four nucleons outside a core to predict cluster rotational bands.[18] This approach appears highly successful for light nuclei and could open up an interesting area of research with heavy-ion beams.

I now wish to discuss a method of combining the high selectivity of the heavy-ion reaction, with the simplicity of the differential cross sections and with a study of the energy variation over a wide range to select systematically states of progressively higher spin in the rotational band. A good example is the $^{12}C(^{12}C,^{9}Be)^{15}O$ reaction[19] for which we show a spectrum at 187 MeV in Fig. 9. The pronounced excitation of states at 12.87 and 15.08 MeV is reminiscent of single particle states in a(d,p) spectrum. The J^{π} values for these states have been assigned tentatively from various systematics.[16] The energy variation of the cross sections in Fig. 10 shows that at the lowest energy of 78 MeV the cross section for states of $J^{\pi} = 1/2^{-}$, $5/2^{+}$ and $13/2^{+}$ are comparable, whereas at 187 MeV, there is a ratio $\approx 10^{3}$ between $13/2^{+}$ and $1/2^{-}$ states. This observation, if accounted for by reaction dynamics, can be used to infer J^{π} values.

The full quantum mechanical calculation of three nucleon transfer at high energies, dominated as it is by recoil effects, is difficult. Here we use a semiclassical expression for the transition probability[16] from an initial state with orbital and magnetic quantum numbers $(\ell_1\lambda_1)$ to a final state $(\ell_2\lambda_2)$:

$$P \alpha \left| Y_{\ell_1}^{\lambda_1}\left(\frac{\pi}{2},0\right) Y_{\ell_2}^{\lambda_2}\left(\frac{\pi}{2},0\right) \right|^2 \; EXP\left[-\left(\frac{R\Delta k}{\pi}\right)^2 - \left(\frac{\Delta L}{\sqrt{\gamma R}}\right)^2\right] \tag{10}$$

where $\Delta k = k_o - \frac{\lambda_1}{R_1} - \frac{\lambda_2}{R_2}$, $k_o = {}^{mv}/_{\hbar}$ (11)

$$\Delta L = (\lambda_2 - \lambda_1) + 1/2\, k_o\, (R_1 - R_2) + {}^{QR}/_{\hbar v} \tag{12}$$

Here $R = R_1 + R_2$, γ is related to an average of the binding energies ε of the initial and final states by $\gamma^2 = \frac{2m\varepsilon}{\hbar^2}$, and m is the transferred mass. The transfer probability is large only if Δk, $\Delta L \approx 0$, and the expressions 11, 12 relate the energy dependence to the J-value of the state via the magnetic substates. Total transition probabilities between states $(j_1 \ell_1)$ and $(j_2 \ell_2)$ are calculated by summing over λ_2 and averaging over λ_1. The comparison of P with the experimental cross sections is made by observing that:

$$\sigma = 2\pi \int \left(\frac{d\sigma}{d\Omega}\right) \sin\Theta d\Theta = \frac{2\pi}{k^2} \int P(L)\, LdL \tag{13}$$

The main contribution to the first integral comes from the maximum of $({}^{d\sigma}/_{d\Omega}) \sin\Theta$ (remembering that ${}^{d\sigma}/_{d\Omega}$ decreases monotonically) and to the second from P(L) for the grazing orbit. These considerations form the basis for our comparison of P and ${}^{d\sigma}/_{d\Omega}$ in Fig. 10.

The theory provides confirmatory evidence for the high spin assignment of the $13/2^+$ state and also (not shown) for the $11/2^-$ state. The folding potential model[18] for the motion of ^{3}He outside the ^{12}C core predicts $13/2^+$ and $11/2^-$ states (which are the upper members of "rotational bands" with $2N + L = 6$ and 5 respectively) at excitations close to the observed states. A further interesting case, beyond the range of the present experiment, is the $11/2^+$ and $9/2^-$ members of the rotational bands, which are the components of the $13/2^+$ and $11/2^-$ states, raised by the ^{3}He spin-orbit potential to over 20 MeV in excitation.

The folding potential model for a rotational band is more transparent in the absence of the spin-orbit potential, eg. for $^{20}Ne \rightarrow {}^{16}O + \alpha$, when we can write[18]:

$$V(r) = -\frac{2\pi\hbar^2}{M}\,\bar{f}\int d^3\underline{r}'\;\rho_{^{16}O}\,(\underline{r}-\underline{r}')\;\rho_{\alpha}\,(\underline{r}')\;dr' \qquad (14)$$

In Fig. 11 this potential is compared with the conventional Saxon-Woods potential for the g.s. rotational band of ^{20}Ne, whose depth must be adjusted to fit the binding energy of each state. The one-particle Shroedinger equation in V(r) is solved for the states specified by N and L, which are related to the n_i and ℓ_i of the particles making up the cluster by:

$$2N + L = \sum_{1}^{n_c} 2\,n_i + \ell_i \qquad (15)$$

where n_c is the number of particles in the cluster. On the right of Fig. 11 are the predicted 2N + L = 8 and 9 rotational bands of ^{16}O compared with experiment.[18] The 8^+ and 9^- members of these bands have not so far been discovered, but a promissing line of attack might be the energy variation of the $^{16}O(^{20}Ne,{}^{16}O)^{16}O$ reaction. The predicted variation for these bands is shown in Fig. 12, and at the highest energy the states separate in order of increasing J-values.

Although the semiclassical analysis presented here represents an extreme oversimplification it is valuable for making wide and rapid surveys in order to see where lie the interesting areas for experimental investigation. It is worth noting however that many of the interesting states discovered, and awaiting discovery, are high spin states of small binding energy, or even unbound. In the limit of small binding energy, defined by $\chi_2 R_1 << 1$, where

$\chi_2 = \sqrt{\frac{2m\varepsilon_2}{\hbar^2}}$, ε_2 being the binding energy of m in the final state and R_1 the radius of the projectile, Nagarajan has shown[20] that the reaction proceeds almost entirely via the recoil momentum transfer, and that the 6D- integration of finite-range DWBA approximates to:

$$\int \underline{dr}_1 \, e^{-\underline{k}_R \cdot \underline{r}_1} \, V(r_1) \, U_{\ell_1}(r_1) \int d\underline{r} \, e^{i\underline{q}\cdot\underline{r}} \, h_{\ell_2}(i\chi_2 r) \times \Theta(r) \qquad (16)$$

where $U_{\ell_1}(r_1)$ is the initial radial wave function and the final weakly bound wave function is approximated by a Hankel function. $\Theta(r)$ is an amplitude modulation of the plane waves to simulate distorted waves. Further $q = \underline{k}_i - \underline{k}_f$ is related to the reaction Q-value of Equ. 12, and $\underline{k}_R$ is proportional to $\underline{k}_o$, the recoil momentum transfer, so the approximation represented by Equ. 16 has a structure paralleling the expression for the semiclassical transition probability of Equ. 10, both justifying the use, and possibly accounting for the success, of the semi-classical theory.

5. Compound or Direct Multinucleon Transfer?

The desirability of extending the above studies to more massive transfers and to more exotic nuclear structures is obvious. There is however overwhelming evidence that even at the highest energy, reactions involving the transfer of more than four nucleons proceed by compound nuclear formation[21], with angular distributions corresponding to the limit $\Theta_g \Delta\ell \to 0$ of Fig. 4. This distribution is of the form $1/\sin\Theta$ characteristic of the decay of a high spin compound nucleus. The example of $^{12}C(^{14}N,^{6}Li)^{20}Ne$ at 76 MeV in Fig. 13 represents the highest energy studied and also the first data for which complete angular distributions were measured.[22] The theoretical curves are Hauser-Feshbach calculations.[23]

The comparison of energy spectra for this reaction at 76 and 120 MeV in Fig. 14 shows that the compound nuclear reaction selectively excites high spin states at the lower energy, whereas at 120 MeV no pronounced excitations are observed at all above the continuum. This feature has been accounted for in the Hauser-Feshbach calculations of Klapdor et al.[24,25]

Physically the reasons are as follows. The most likely spin I to be populated in the final nucleus is the difference between J_i, the maximum angular momentum in the entrance channel for which compound nuclear formation can occur, and J_f the grazing angular momentum carried off for residual excitation E_x. If we estimate the density of levels ρ with $J \geqslant J_i - J_f$, then (i) if no levels of spin J are present at E_x, the cross section will be vanishingly small, but (ii) if the density is small but finite a selective population will be observed and (iii) if the density is very large, the reaction will exhibit no selectivity. These conditions can account quantitatively for the differences in the spectra of Fig. 14.

These compound reactions are of course interesting for spectroscopy in their own right. For example, an important ingredient in the Hauser-Feshbach calculation is the cut-off angular momentum in the compound nucleus[26], since frequently the heavy-ions bring in more angular momentum than the compound system can support before fission.[27] In the (^{14}N, ^{6}Li) reaction at 76 MeV the best agreement with the magnitude of the experimental cross sections was achieved[21,23], when the total angular momentum was limited to 18$\hbar$ compared to the grazing angular momentum of 21$\hbar$. Although the value of 18$\hbar$ agrees with some theoretical models for limiting angular momenta[21], there is also the possibility that the yrast line in the compound nucleus is the limiting factor.

The interesting question now is whether we can marshall the above criteria to help us choose a multinucleon transfer reaction, in which the direct amplitude might again be large. An idea of the selectivity expected in the $^{12}C(^{20}Ne,\alpha)^{28}Si$ reaction at 100 MeV is conveyed by Fig. 15, adapted from the approach of Klapdor et al.[25] It shows the locus of preferred excitations in the residual nucleus, computed from the difference between the angular momentum carried into the compound nucleus in a grazing collision,

$$\sqrt{L(L+1)}\ \hbar = 2\hbar\eta\ \frac{E_{CM}}{V_C^i}\left(1 - \frac{V_C^i}{E_{CM}}\right)^{1/2} \qquad (17)$$

of $22\hbar$, and the angular momentum removed by the outgoing α of energy $E_f = (E_{CM} + Q - E_x)$. This curve has a vertex corresponding to a final energy equal to the Coulomb barrier in the exit channel, i.e. at:

$$E_x = E_{CM} + Q - V_C^f \qquad (18)$$

The density of levels in the residual nucleus ^{28}Si is shown on the figure, calculated from the formula[28]:

$$\rho(U,I) = \frac{(2I+1)}{12\sqrt{2}\ a^{1/4}\ U^{5/4}\ 2\sigma^3}\ EXP(2\sqrt{aU})\ EXP\left[-(I+1/2)^2/2\sigma^2\right]$$

where suitable values of the level density parameter "a" and the spin cut-off parameter "σ" are discussed in Refs. 21,25. Also shown is the yrast line for ^{28}Si, obtained from the expression:

$$E_y = \frac{\hbar^2 J^2}{2\mathcal{J}} \qquad (21)$$

where $\mathcal{J}$ was taken as 0.5 times the rigid body moment of inertia ($2/5\ m\ R^2$, $R = R_o A^{1/3}$ with $R_o = 1.4$ fm) at low excitations, increasing to the rigid body value at high excitation.

The locus of preferred excitations in the region of 15 - 30 MeV excitation lies well above the yrast line, cutting through a region of high level density. It should be noted that if the effect of nuclear deformation is taken into account the yrast line will be lower on the diagram. On account of the arguments above, this reaction would not be expected to be selective from a compound nuclear mechanism. A spectrum for this reaction is given in Fig. 16, in which we do see selective excitation of states with $d\sigma/d\Omega \approx 100$ μb/sr. Since ^{20}Ne has a large spectroscopic probability for dissociation into ^{16}O + α, it is possible that these states are formed by direct transfer of the ^{16}O nucleus, and the residual states could be candidates for quasimolecular configurations in ^{28}Si. So far such states have been observed as resonances in the excitation functions for elastic scattering[29] of ^{12}C on ^{16}O or of related transfer reactions,[30,31] which generally span a higher region of excitation than is covered in the present experiment. However, the two states observed strongly in ^{16}O(^{16}O,α)^{28}Si reaction[32] do not agree precisely with any of our observed excitations. If quasimolecular states can be observed as residual states in transfer reactions, we have at our disposal a flexible technique for studying their properties in much the same way that the study of doorway states was transformed by observing them as residual three quasi-particle states in transfer reactions rather than intermediate resonances in excitation functions. Further work is required on the (^{20}Ne,α) reaction to rule out definitively the possibility of compound nuclear contributions by measuring angular distributions and calculating Hauser-Feshbach cross sections.

6. Conclusion

In this talk I have used some simple properties of differential cross sections in high energy heavy-ion reactions to focus on possible new aspects of reaction mechanisms and nuclear structure. Inevitably in any field in which there was another peak of activity almost twenty years ago, there is a tendency to rediscover old ideas. Some of my talk may be summarized in the old proverb about "serving new wine in old bottles" or more appropriately of serving old wine in new bottles." Nevertheless it is the impetus of the new wave of research results from Cyclotrons and high energy Tandems that have sharpened and focussed these ideas. The data even at this stage are still rather crude and sparse but they are certainly suggestive of a promissing future for heavy-ion reactions on the machines under construction.

Acknowledgements

The ideas discussed in this talk have been mainly developed around experiments conducted on the 88-Inch Cyclotron over the last year, done in collaboration with the experimental group of B. G. Harvey, D. L. Hendrie, U. Jahnke, L. Kraus, C. F. Maguire, J. Mahoney, Y. Terrien and K. Yagi; and with the theoretical group of N. K. Glendenning, G. Delic and G. Wolschin. I also wish to thank the other research groups, mentioned in the text, whose work and ideas I have used, in particular B. Buck, and H. V. Klapdor for communicating results prior to publication, and J. Millener for making the semiclassical calculations for the (^{20}Ne,^{16}O) reaction. Finally I thank D. M. Brink for the influence of many discussions and lectures.

REFERENCES

0. T. Kammuri, Prog. Th. Phys. 28 (1962) 934.

1. V. M. Strutinskii, Sov. Phys. JETP 19 (1964) 1401; Phys. Lett. 44B (1973) 245.

2. W. A. Friedman, K. W. McVoy, and G. W. T. Shuy, Phys. Rev. Lett. 33 (1974) 308.

3. T. Suzuki, Prog. Th. Phys. 41 (1969) 695.

4. S. Kahana, P. D. Bond, and C. Chasman, Phys. Lett. 50B (1974) 199.

5. R. J. Ascuitto and N. K. Glendenning, Phys. Lett. 48B (1974) 6.

6. A. G. Artukh, G. F. Gridnev, V. L. Mikheev, V. V. Volkov, and J. Wilczynski, Nuc. Phys. A215 (1973) 91.

7. For a recent review, see A. Fleury and J. M. Alexander, Ann. Rev. Nuc. Sci. 24 (1974) 279.

8. D. K. Scott, B. G. Harvey, D. L. Hendrie, U. Jahnke, L. Kraus, C. F. Maguire, J. Mahoney, Y. Terrien, K. Yagi, N. K. Glendenning, to be published.

9. N. Anyas-Weiss, J. C. Cornell, P. S. Fisher, P. N. Hudson, A. Menchaca-Rocha, A. D. Panagiotou, I. Paschopolous, and D. K. Scott, Proceedings of the International Conference on Nuclear Physics, eds. J. de Boer and H. J. Mang (North-Holland, 1973) Vol. 1, p. 485.

10. R. J. Ascuitto and N. K. Glendenning, Phys. Lett. B47 (1973) 33.

11. O. Beer, A. El Behay, P. Lopato, Y. Terrien, G. Vallois, and K. Seth, Nuc. Phys. A147 (1970) 326.

12. P. H. Stelson and L. Grodzins, Nuc. Data A1 (1966) 21.

13. See also K. A. Erb, D. L. Hanson, R. J. Ascuitto, B. Sorensen, J. S. Vaagen, and J. J. Kolata, Phys. Rev. Lett. 33 (1974) 1102.

14. For a recent review, see J. D. Garrett in Proceedings of the Symposium on Classical and Quantum Mechanical Aspects of Heavy-Ion Collisions, (Heidelberg, 1974) to be published.

15. J. Birnbaum, J. C. Overley and D. A. Bromley, Phys. Rev. 157 (1967) 787.

16. N. Anyas-Weiss, J. C. Cornell, P. S. Fisher, P. N. Hudson, A. Menchaca-Rocha, D. J. Millener, A. D. Panagiotou, D. K. Scott, D. Strottman, D. M. Brink, B. Buck, P. J. Ellis, and T. Engeland, Phys. Reports, 12C (1974) 203.

17. L. R. Dodd and K. R. Greider, Phys. Rev. 180 (1968) 1187.

18. B. Buck, C. B. Dover and J. P. Vary, to be published.

19. D. K. Scott, D. L. Hendrie, U. Jahnke, L. Kraus, C. F. Maguire, J. Mahoney, Y. Terrien, and K. Yagi, to be published.

20. M. A. Nagarajan, Phys. Lett. 52B (1974) 395.

21. For a recent review, see R. Stokstad, in Proceedings of the International Conference on Reactions between Complex Nuclei, eds. R. L. Robinson, F. K. McGowan, J. B. Ball, and J. H. Hamilton (North-Holland, 1974) Vol. 2, p. 327.

22. T. A. Belote, N. Anyas-Weiss, J. A. Becker, J. C. Cornell, P. S. Fisher, P. N. Hudson, A. Menchaca-Rocha, A. D. Panagiotou, and D. K. Scott, Phys. Rev. Lett. 30 (1973) 450.

23. D. Hanson, R. G. Stokstad, K. A. Erb, C. Olmer, and D. A. Bromley, Phys. Rev. C 9 (1974) 929.

24. H. V. Klapdor, H. Reiss, and G. Rosner, Phys. Lett. 53B (1974) 147.

25. H. V. Klapdor, G. Rosner, H. Reiss, and M. Schrader, Nuc. Phys. to be published.

26. C. Volant, M. Conjeaud, S. Harar, A. Lepine, E. Frota da Silveira, and S. M. Lee, Nuc. Phys. A238 (1975) 120.

27. W. J. Swiatecki, J. Phys. (Paris) 33 (1972) C5-45.

28. A. Gilbert and A. G. W. Cameron, Can. J. Phys. 43 (1965) 1446.

29. A. Gobbi, R. Weiland, L. Chua, D. Shapira, and D. A.Bromley, Phys. Rev. C 7 (1973) 30.

30. P. T. Debevec, H. J. Korner, and J. P. Schiffer, Phys. Rev. Lett. 31 (1973) 171.

31. D. J. Crozier and J. C. Legg, Phys. Rev. Lett. 33 (1974) 782.

32. W. R. Wharton, P. T. Debevec, and J. P. Schiffer, Proceedings of the International Conference on Nuclear Physics, eds. J. de Boer and H. J. Mang, (North-Holland, 1973) Vol. 2, p. 541.

FIGURE CAPTIONS

1. The relation between $\Delta\theta$ and $\Delta\ell$ predicted from equ. 7. The curve labelled Qu. Mech. is obtained by setting the second dispersive term in equ. 7 to zero. For small $\Delta\ell$ values the curves coincide, but for large $\Delta\ell$ (the classical region) they diverge.

2. Differential cross sections for one- and two-neutron pick-up induced by ^{12}C on ^{144}Nd at 78 MeV. For $(^{12}C,^{13}C)$ two sets of DWBA calculations are shown; the solid line is for V = -40, W = -15, r_0 = 1.31, a_0 = 0.45, and the dotted line is for V = -100, W = -40, r_0 = 1.22, a_v = 0.49, a_w = 0.6. The classical maximum is stable against this variation. For $(^{12}C,^{14}C)$ we compare two calculations with the V = -40 MeV potential with r_0 = 1.36 fm (dotted) and 1.26 fm (solid). The cross section is highly sensitive to this variation.

3. The reaction amplitude for $(^{12}C,^{14}C)$ reaction on ^{144}Nd is shown on the left for the two potentials discussed in Fig. 2. On the right are shown the corresponding optical model deflection functions obtained by differentiating the DWBA phase shifts.

4. On the left are shown the universal distribution curves for a peripheral reaction, based on the complete form of equ. 6 (see ref. 1), illustrating the transition from bell-shape to monotonic decrease. This trend closely resembles the experimental data for reactions of ^{40}Ar + ^{232}Th at 389 MeV on the right (ref. 6).

5. Differential cross sections for the reactions $^{120}Sn(^{18}O,^{16}O)^{122}Sn$ at 99 MeV and $^{122}Sn(^{16}O,^{18}O)^{120}Sn$ at 104 MeV. The solid lines are the CCBA predictions for $(^{18}O,^{16}O)$ and the dashed lines for $(^{16}O,^{18}O)$. For the $(^{18}O,^{16}O)$ reaction the open symbols represent counter telescope data of ref. 9.

6. Illustration of the amplitudes relevant to two-neutron transfer involving direct and indirect modes, as discussed in the text.

7. The differential cross sections for elastic and inelastic scattering (2^+) of ^{16}O on ^{122}Sn at 104 MeV. The curves are the predictions of coupled channels theory.

8. Collected differential cross sections for one, two, and three-nucleon transfer reactions on light nuclei induced by heavy-ion beams of approximately 10 MeV/nucleon. The data are plotted against the square of the linear momentum transfer q to remove kinematic differences. The theoretical lines q^{-3} and q^{-4} are based on an approximate recoil DWBA calculation (ref. 17).

9. Energy spectra for the $^{12}C(^{12}C,^{9}Be)^{15}O$ reaction at 187 MeV showing the selective excitation of postulated high-spin states $13/2^+$ and $11/2^-$.

10. The energy variation of the cross section for states excited in the $^{12}C(^{12}C,^{9}Be)^{15}O$ reaction. The solid curves are the predictions of semi-classical theory (no spectroscopic factors included).

11. Single particle Saxon-Woods potentials appropriate to the ground state band of ^{20}Ne, viewed as $\alpha + ^{16}O$. The depth was adjusted separately for for each state to fit the binding energy. The dashed curve represents the folded potential of equ. 14 with $\bar{f} = 1.237$ fm. At the right are the $K^{\pi} = 0^{+}$ and 0^{-} rotational bands in ^{16}O, where the theoretical energies were obtained as bound states and resonances of the $\alpha + ^{12}C$ folded potential with $\bar{f} = 1.425$ fm for the 0^{+} band and 1.55 fm for the 0^{-}.

12. The energy variation predicted by the semiclassical model (equ. 10), for the reaction $^{12}C(^{20}Ne,^{16}O)^{16}O$ to the $K^{\pi} = 0^{+}$ and 0^{-} rotational bands.

13. Differential cross sections for selectivily excited states in the $^{12}C(^{14}N,^{6}Li)^{20}Ne$ reaction at 76 MeV. The distributions follow approximately a $1/\sin\theta$ form, which is reproduced by the Hauser-Feshbach calculations (ref. 23).

14. Energy spectra for the $^{12}C(^{14}N,^{6}Li)^{20}Ne$ reaction at 76 MeV (top) and 120 MeV(bottom), showing the loss of selectivity at the higher energy.

15. Preferred locus of excitation in the $^{12}C(^{20}Ne,\alpha)^{28}Si$ reaction calculated as the difference $(L_{^{20}Ne} - L_{\alpha})$ for grazing collisions. For comparison the level density in ^{28}Si is shown, and also the yrast line.

16. Energy spectrum for the $^{12}C(^{20}Ne,\alpha)^{28}Si$ reaction at 100 MeV and 8^{o}, showing the selective excitation of states between 16 and 30 MeV.

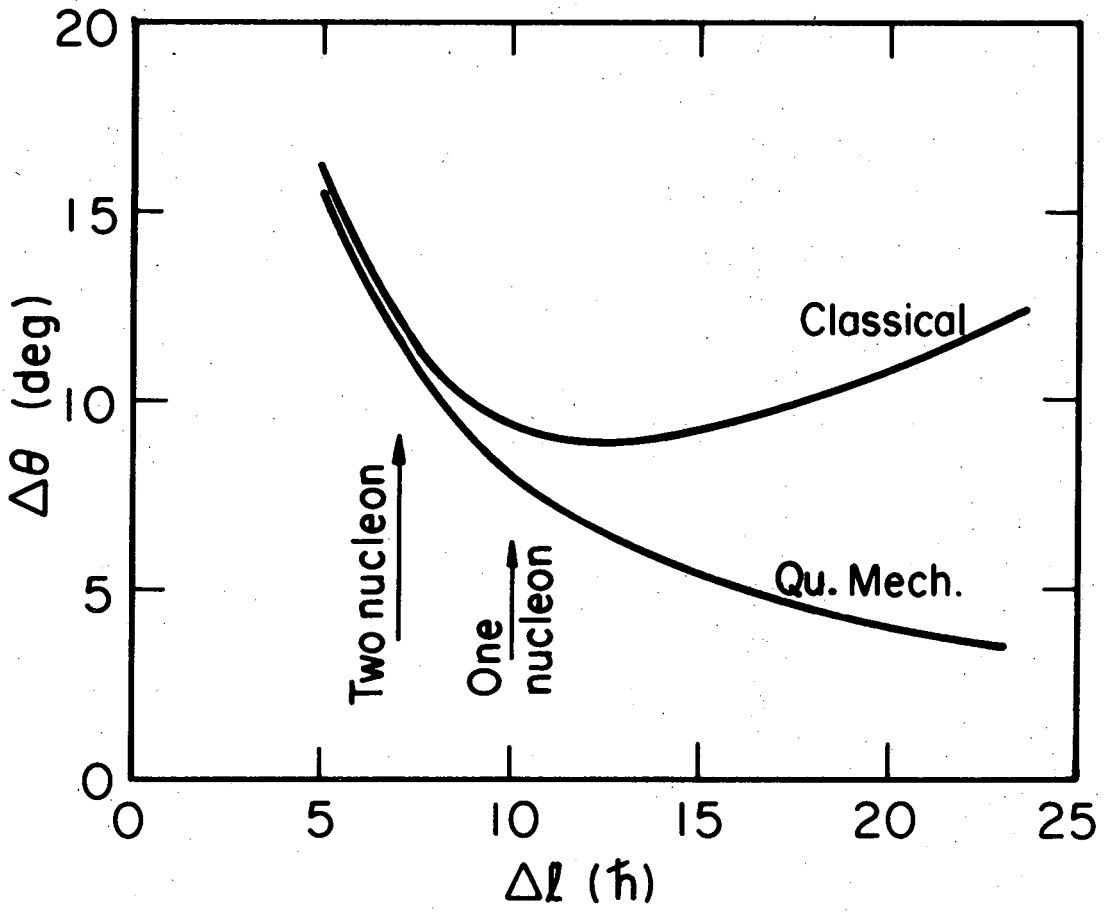
20
15
10
5
0
0
5
10
15
20
25
Δθ (deg)
Δℓ (ħ)
Classical
Qu. Mech.
Two nucleon
One nucleon
XBL752-2266

Fig. 1

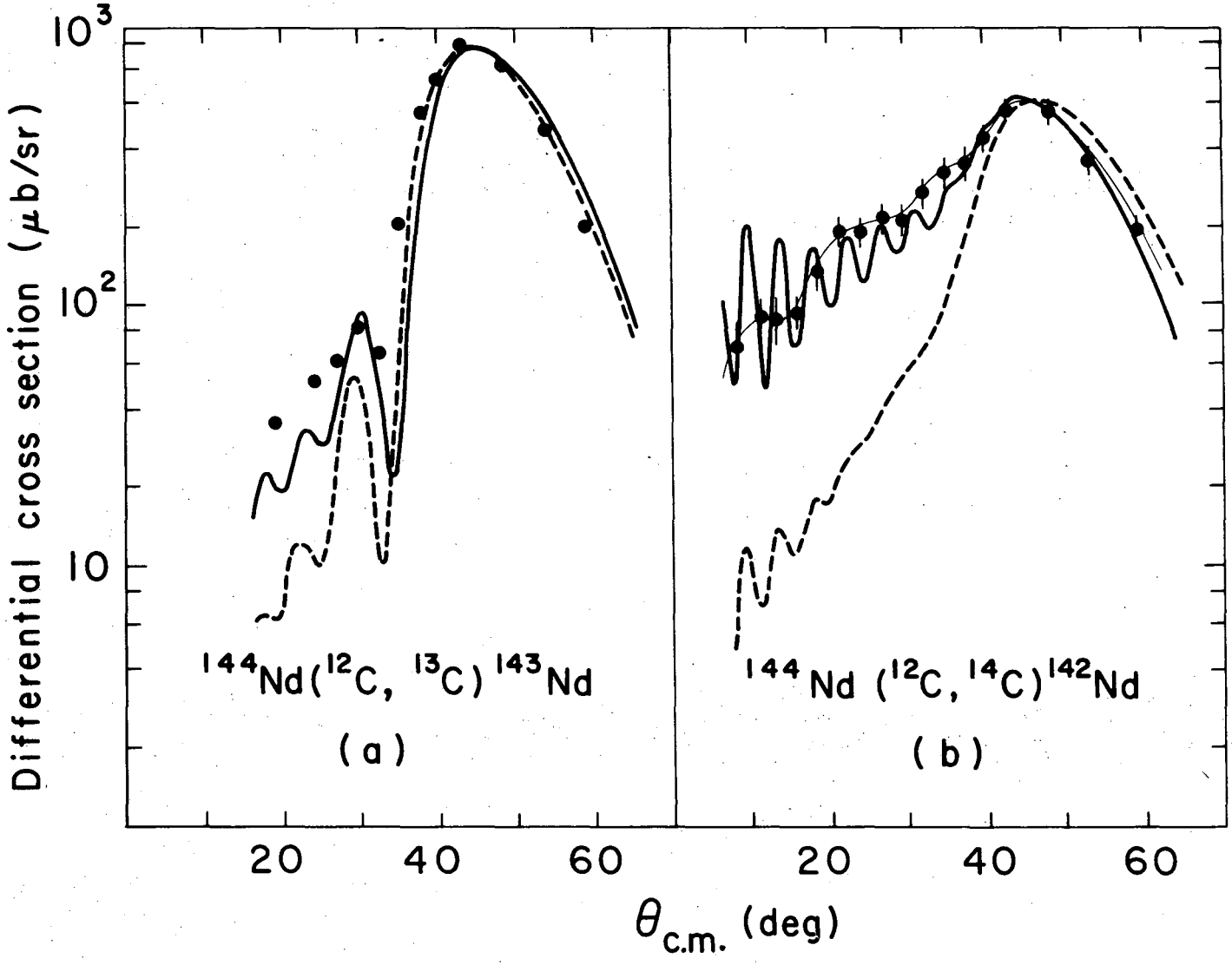
Differential cross section (μb/sr)
10³
10²
10
144Nd(12C, 13C)143Nd
(a)
144Nd (12C, 14C)142Nd
(b)
20
40
60
θc.m. (deg)
XBL752 - 2268

Fig. 2

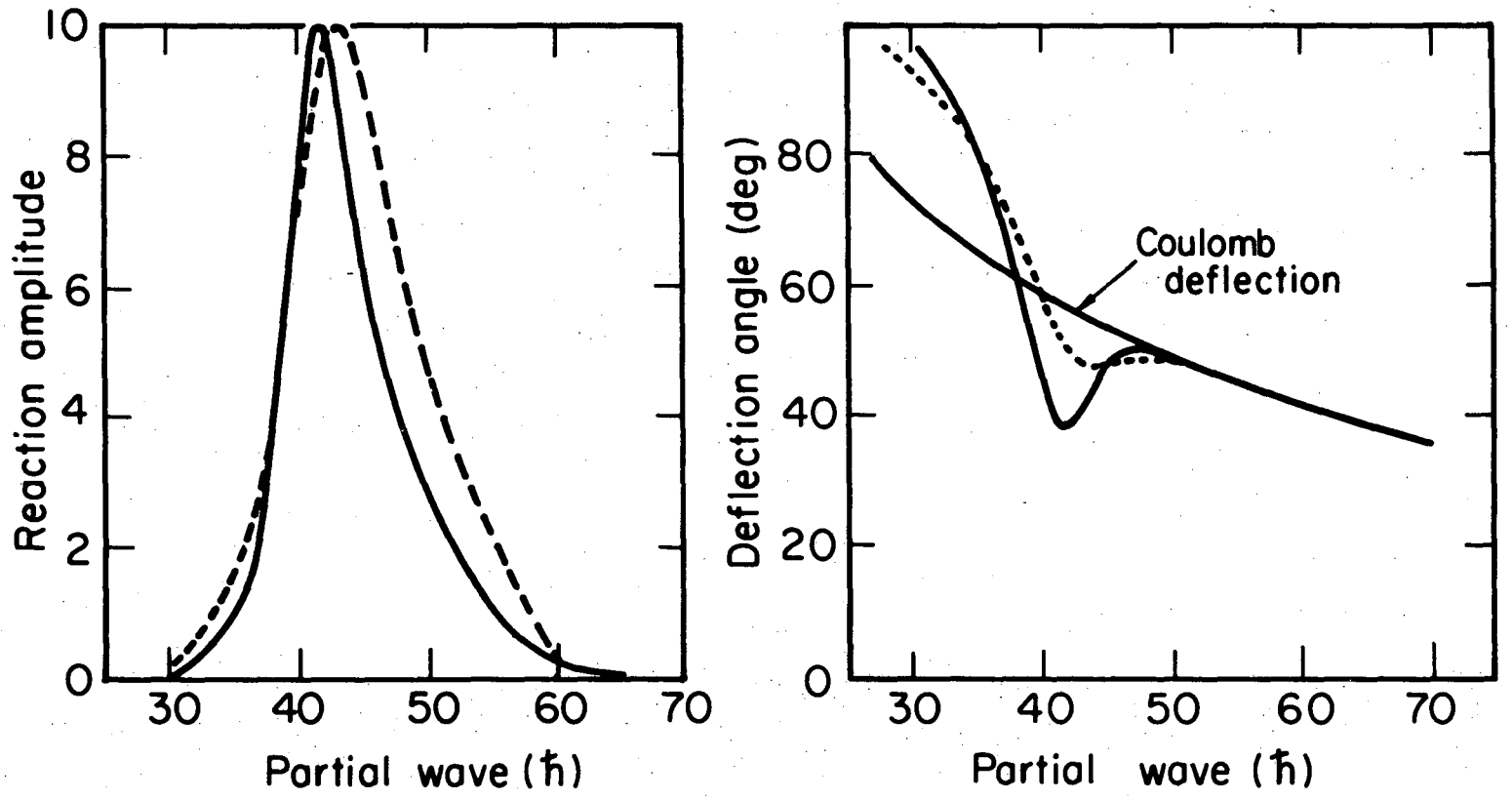

XBL752-2271

Fig. 3

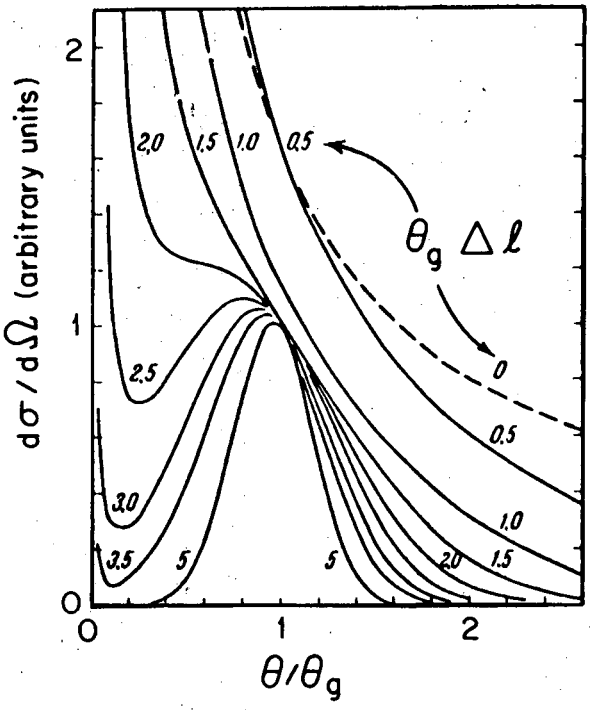

Universal curves for distribution of peripheral reaction

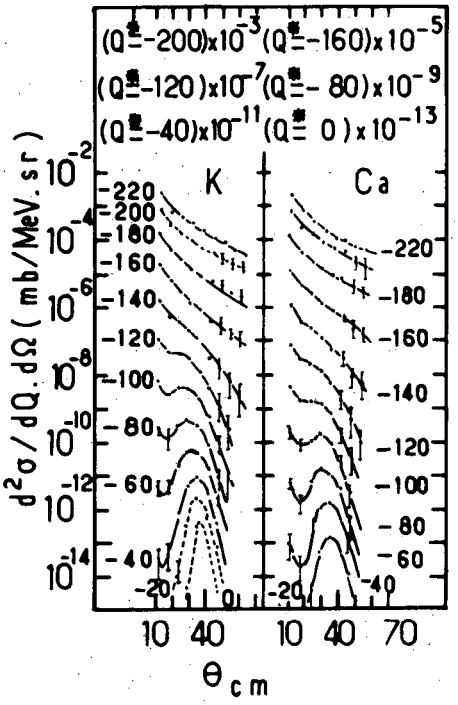

Differential cross sections for $^{40}Ar + ^{232}Th$ at 389 MeV

XBL752-2274

Fig. 4

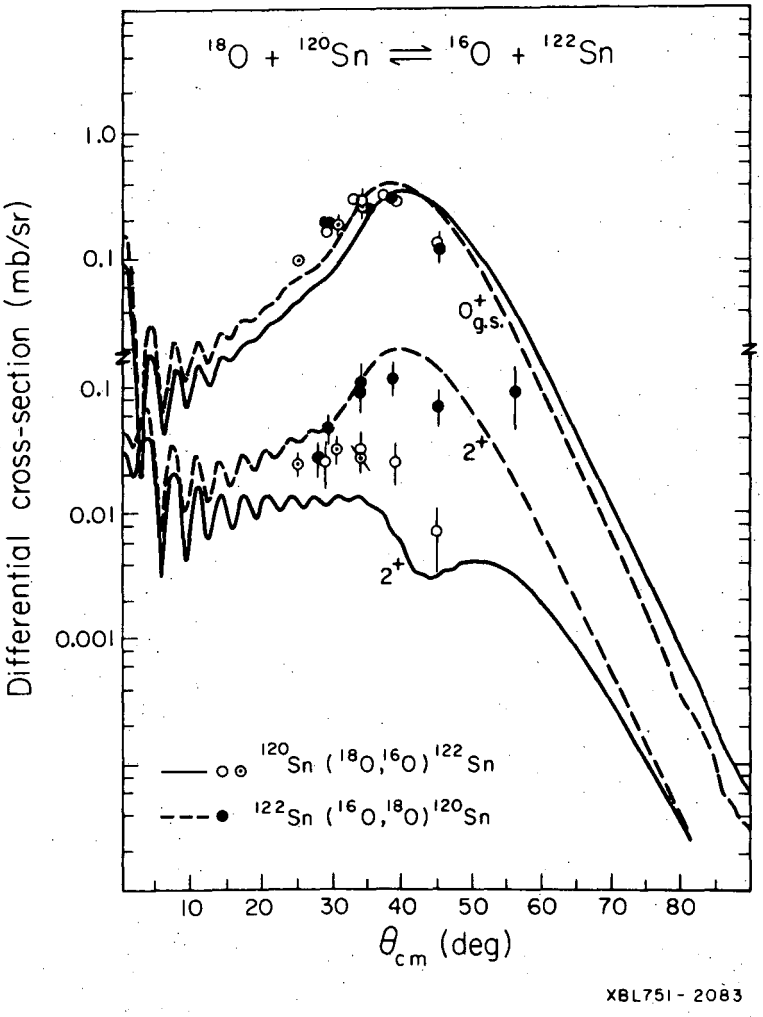
$^{18}O + {}^{120}Sn \rightleftharpoons {}^{16}O + {}^{122}Sn$
Differential cross-section (mb/sr)
1.0
0.1
0.1
0.01
0.001
$0^+_{g.s.}$
2^+
2^+
$^{120}Sn\ (^{18}O,^{16}O)\ ^{122}Sn$
$^{122}Sn\ (^{16}O,^{18}O)\ ^{120}Sn$
10 20 30 40 50 60 70 80
θ_{cm} (deg)
XBL751-2083

Fig. 5

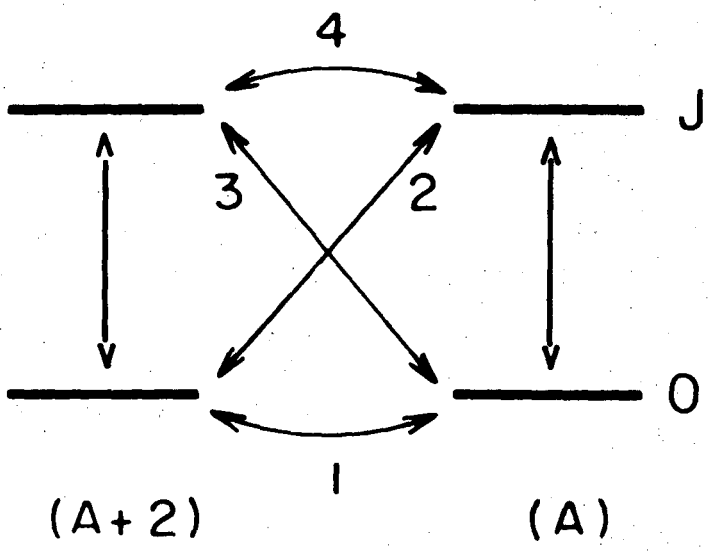

XBL 745-905

Fig. 6

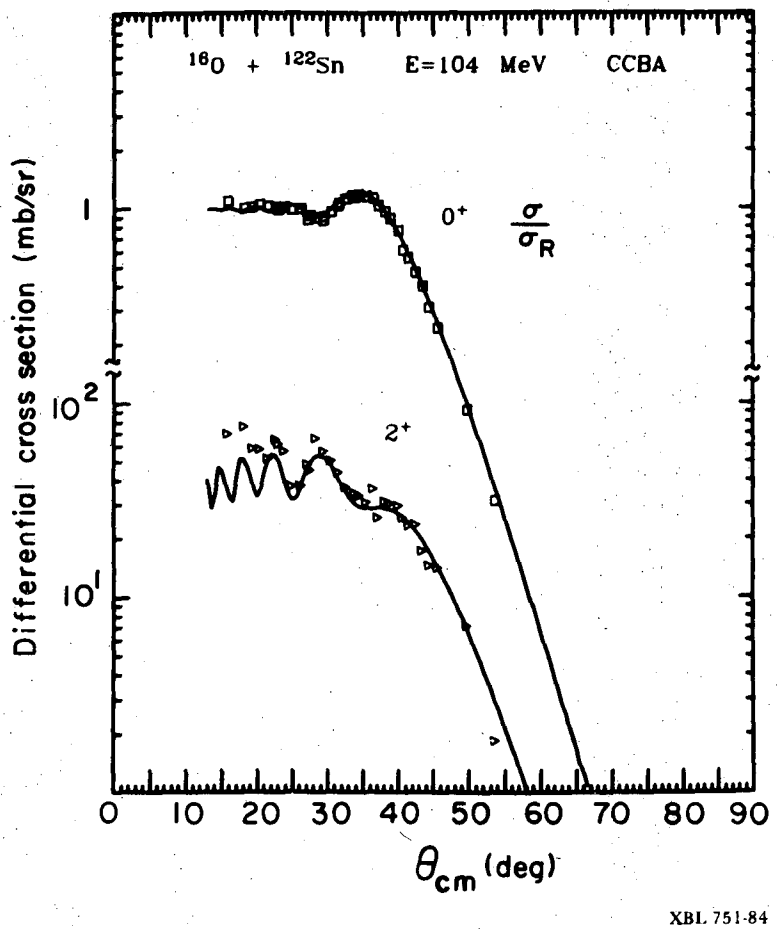
^{16}O + ^{122}Sn E=104 MeV CCBA
0+
$\frac{\sigma}{\sigma_R}$
2+
Differential cross section (mb/sr)
1
10^2
10^1
0 10 20 30 40 50 60 70 80 90
θ_{cm} (deg)
XBL 751-84

Fig. 7

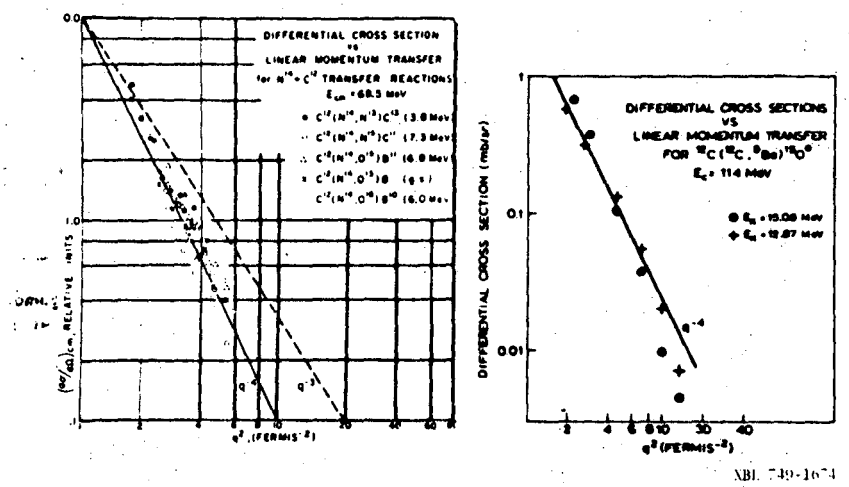
DIFFERENTIAL CROSS SECTION
vs
LINEAR MOMENTUM TRANSFER
for $N^{14}+C^{12}$ TRANSFER REACTIONS
E_{cm} = 68.5 MeV
$C^{12}(N^{14},N^{13})C^{13}$ (3.0 Mev)
$C^{12}(N^{14},N^{13})C^{13}$ (7.3 Mev)
$C^{12}(N^{14},O^{15})B^{11}$ (6.8 Mev)
$C^{12}(N^{14},O^{15})B$ (g.s.)
$C^{12}(N^{14},O^{15})B^{10}$ (6.0 Mev)
q^{-4}
q^{-5}
q^2 (FERMIS^{-2})
DIFFERENTIAL CROSS SECTIONS
VS
LINEAR MOMENTUM TRANSFER
FOR $^{12}C(^{18}C, ^8Be)^{22}O^0$
E_c = 114 MeV
E_x = 15.08 MeV
E_x = 12.87 MeV
q^{-4}
DIFFERENTIAL CROSS SECTION (mb/sr)
q^2(FERMIS^{-2})
XBL 749-1674

Fig. 8

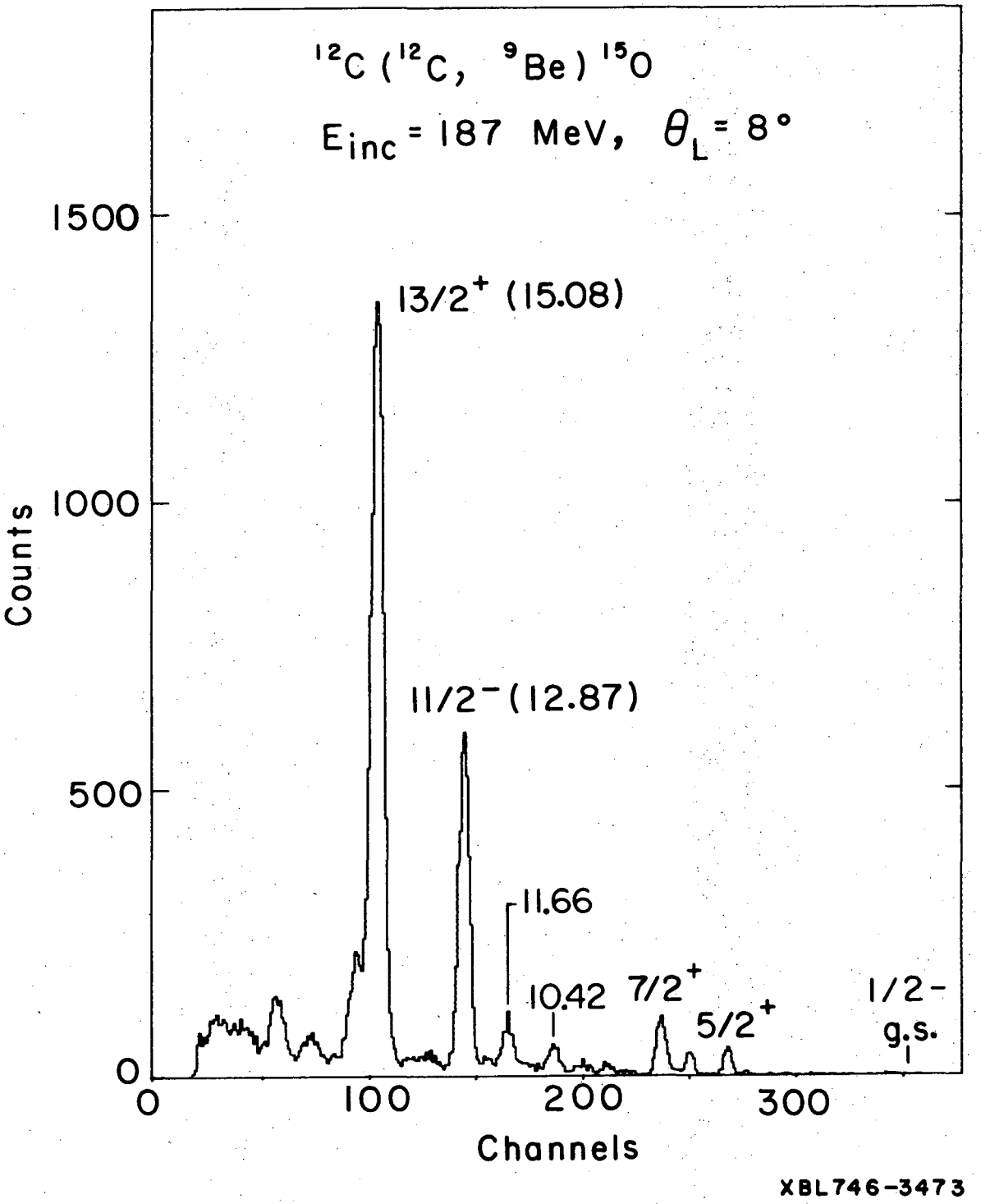
$^{12}C(^{12}C, ^{9}Be)^{15}O$
$E_{inc} = 187$ MeV, $\theta_L = 8°$
1500
1000
500
0
Counts
13/2+ (15.08)
11/2− (12.87)
11.66
10.42
7/2+
5/2+
1/2−
g.s.
0
100
200
300
Channels
XBL746-3473

Fig. 9

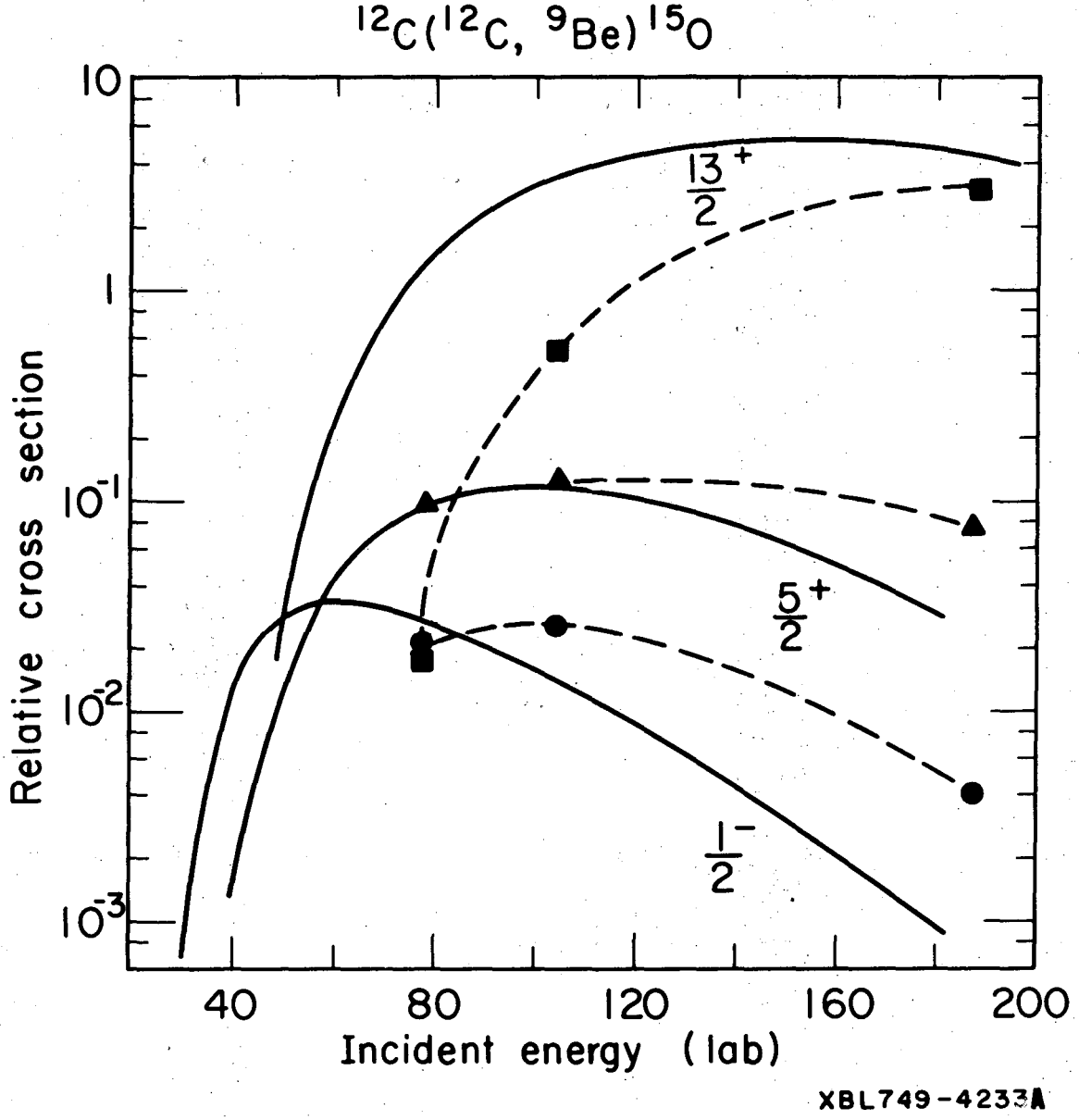

Fig. 10

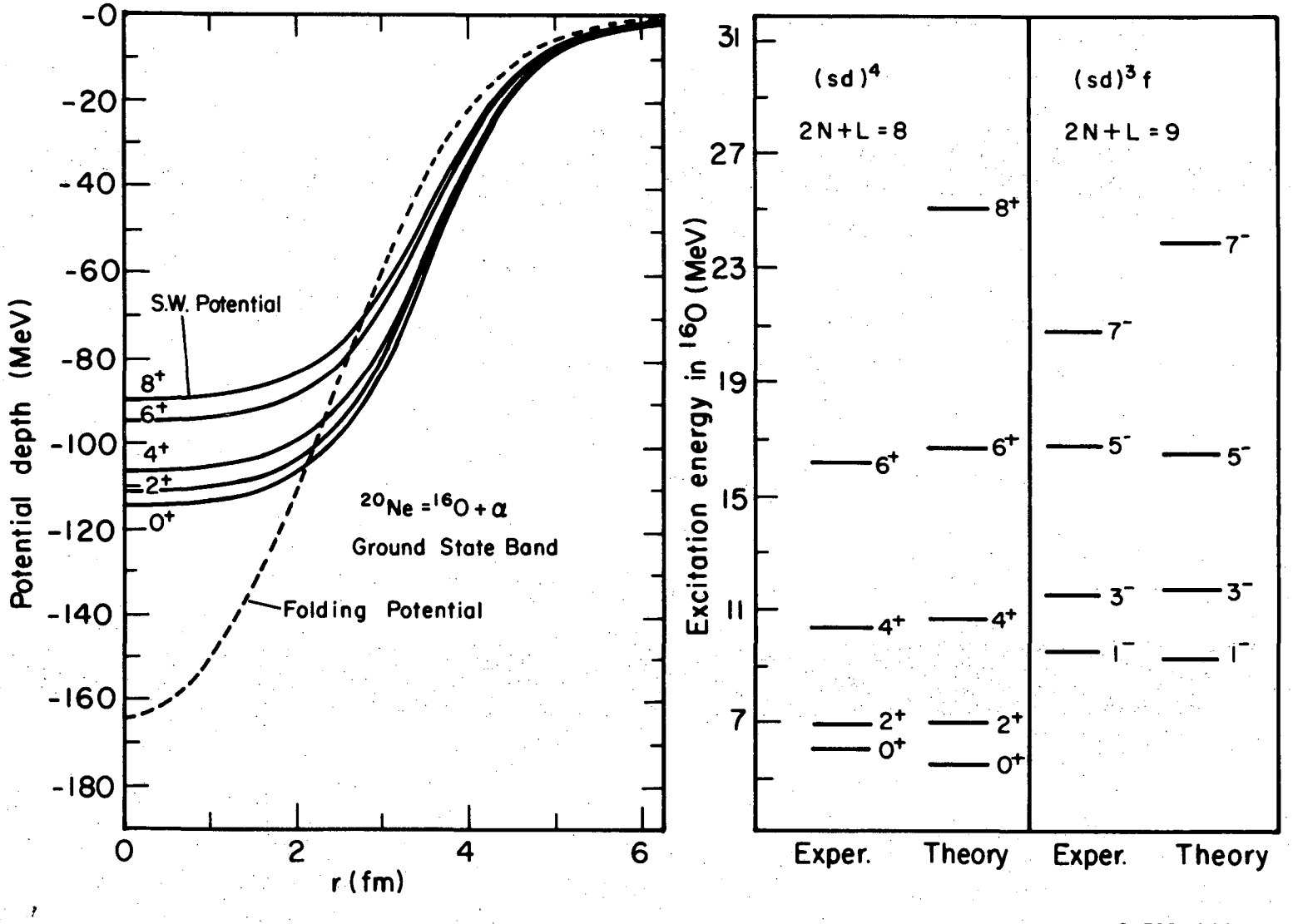
Potential depth (MeV)
-0
-20
-40
-60
-80
-100
-120
-140
-160
-180
S.W. Potential
8+
6+
4+
2+
0+
20Ne = 16O + α
Ground State Band
Folding Potential
0
2
4
6
r (fm)
Excitation energy in 16O (MeV)
31
27
23
19
15
11
7
(sd)4
2N+L = 8
(sd)3 f
2N+L = 9
8+
6+
4+
2+
0+
7-
5-
3-
1-
Exper.
Theory
Exper.
Theory
XBL753-2449

Fig. 11

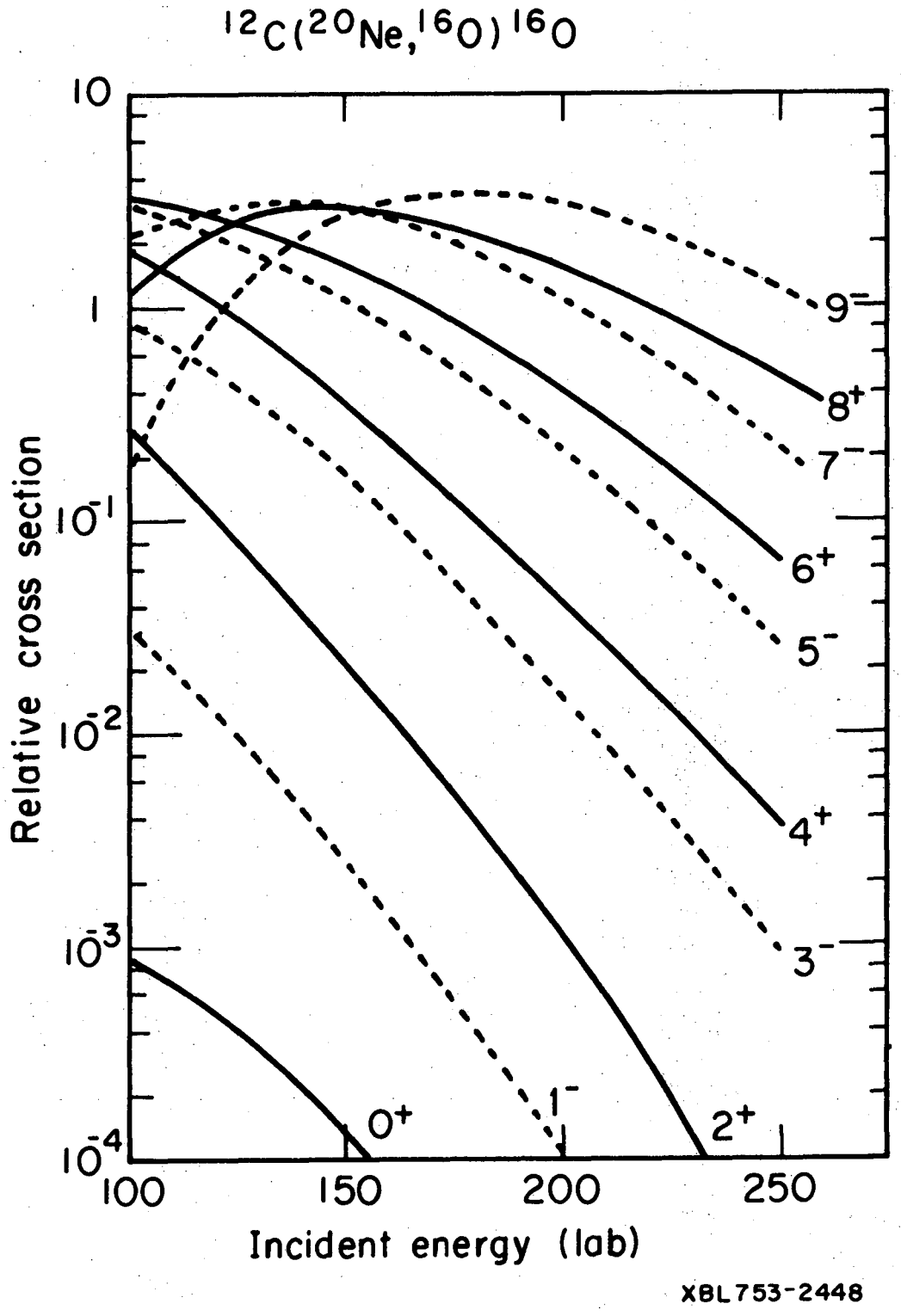
$^{12}C(^{20}Ne,^{16}O)^{16}O$
Relative cross section
10
1
10^{-1}
10^{-2}
10^{-3}
10^{-4}
100
150
200
250
Incident energy (lab)
9^-
8^+
7^-
6^+
5^-
4^+
3^-
1^-
0^+
2^+
XBL753-2448

Fig. 12

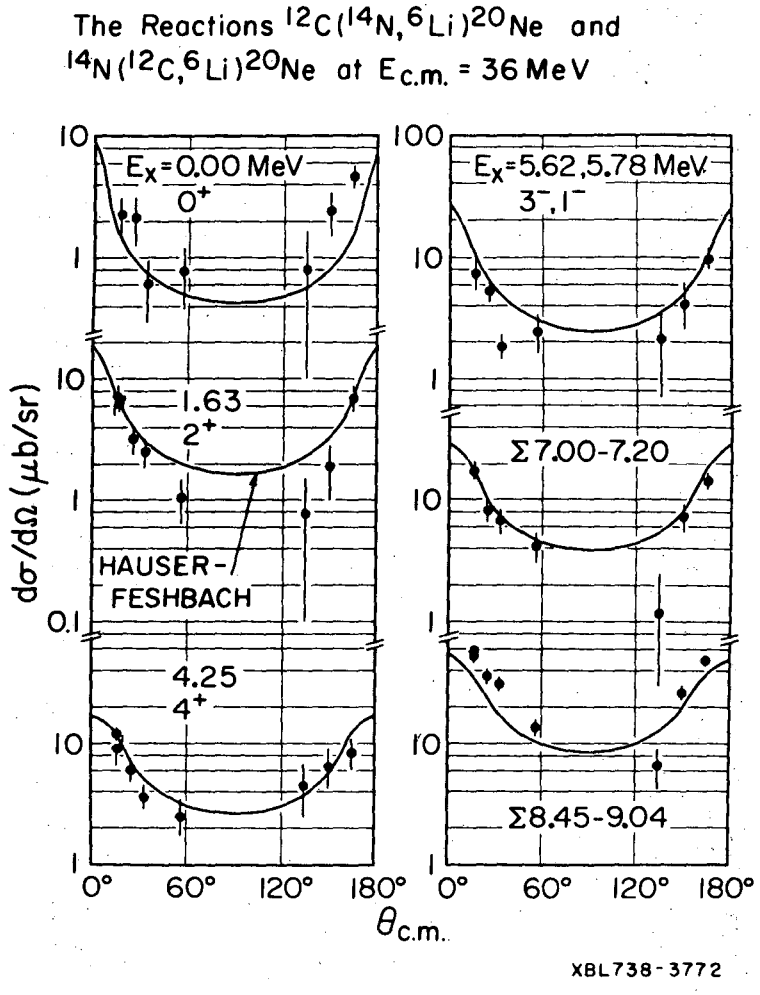
The Reactions $^{12}C(^{14}N,^{6}Li)^{20}Ne$ and
$^{14}N(^{12}C,^{6}Li)^{20}Ne$ at $E_{c.m.}$ = 36 MeV
E_x=0.00 MeV
0^+
1.63
2^+
HAUSER-
FESHBACH
4.25
4^+
E_x=5.62,5.78 MeV
$3^-,1^-$
Σ7.00-7.20
Σ8.45-9.04
$d\sigma/d\Omega$ (μb/sr)
$\theta_{c.m.}$
0°
60°
120°
180°
XBL738-3772

Fig. 13

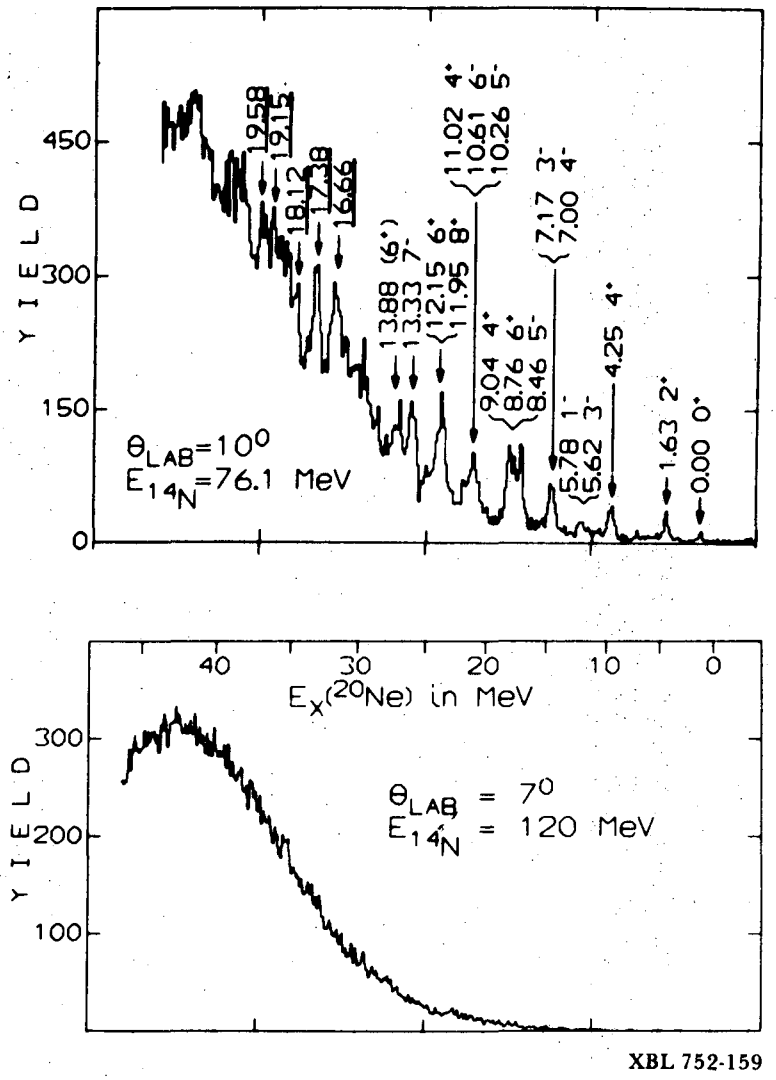

Fig. 14

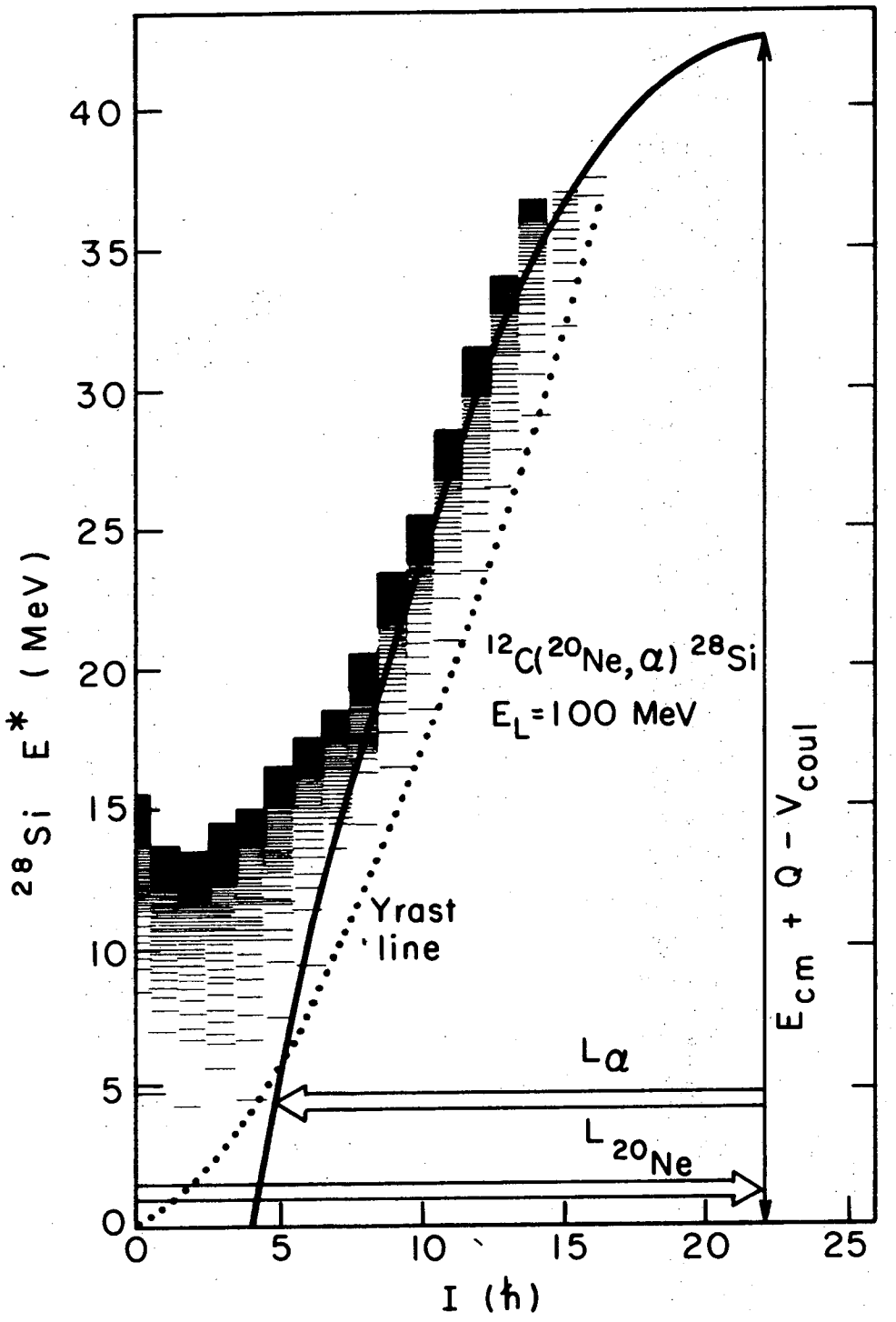

XBL752 -2267

Fig. 15

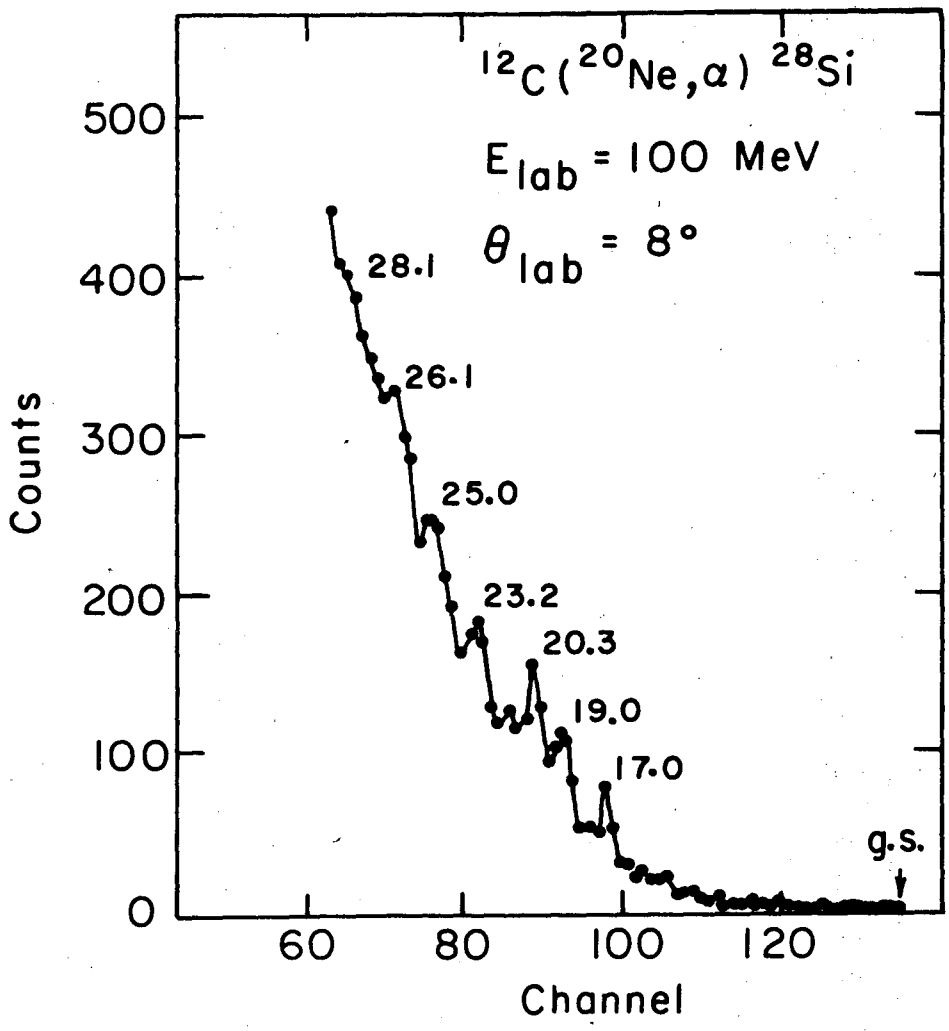

XBL 749-4234

Fig. 16

TECHNICAL INFORMATION DIVISION
LAWRENCE BERKELEY LABORATORY
UNIVERSITY OF CALIFORNIA
BERKELEY, CALIFORNIA 94720